KERNFORSCHUNGSZENTRUM

KARLSRUHE

April 1968

KFK 754

Zyklotron-Laboratorium

Beam Property Measurements at the Karlsruhe Isochronous Cyclotron

D. Hartwig, W. Linder, M.E. Lösel, G. Schatz, H. Schweickert

GESELLSCHAFT FÜR KERNFORSCHUNG M.B.H.

KARLSRUHE

Kernforschungszentrum Karlsruhe

April 1968 K F K - 754

Beam Property Measurements at the Karlsruhe Isochronous Cyclotron

---

D. Hartwig, W. Linder, M.E. Lösel, G. Schatz, H. Schweickert

Kernforschungszentrum Karlsruhe, Zyklotron-Laboratorium

Gesellschaft für Kernforschung mbH., Karlsruhe

1. Introduction

This report summarizes the results of some beam property measurements performed at the Karlsruhe Isochronous Cyclotron. Though probably none of the applied methods is basically new not all of them seem to find widespread use. Due to the limited amount of machine time available for these measurements it was not possible to repeat them frequently, so we are unable to say how critically the results depend on machine parameters. We have no reason to assume, though, that the numbers given are better or worse than the values obtained in routine operation.

2. Measurement of the phase of the internal beam

The phase of the internal beam gives information about the deviations of the mean magnetic field from the design value.

Although 5 capacitive nonintercepting probes for measuring the phase of the internal beam are installed in the Karlsruhe Isochronous Cyclotron[1] two movable targets were built for phase measurements. This was undertaken as the capacitive system

a) averages the phase over several turns due to the radial extension of the pick up probes,
b) is only suitable at currents above approximately 1 μA, and
c) does not extend up to extraction radius.

It should be mentioned, however, that the system has proved extremely useful in routine operation and tune-up of the machine.

Two different probes useful at different levels of current have been developed.

2.1 Description of the probes

2.1.1 High current probe

The high current probe consists of a water cooled block shielded with a tungsten grid to reduce RF pick up.

Fig. 2.1 shows the details of the construction. The cooling water is supplied through two insulating glass tubes in order to keep the capacitance of the beam stop as low as possible (< 6 pF). The copper block is connected to a 100 Ω coaxial cable which is terminated in the target by a 100 Ω resistor. RF shielding is provided by a tungsten grid of 20 µ wire diameter which is pressed to a copper box housing the beam stop. The remaining RF signal on the coaxial cable depends on the target position and has a voltage of $\leq$ 20 mV. It can be compensated by adding an RF voltage coupled from the tank at proper amplitude and phase. The system can then be used from currents between 1 and 30 µA. A typical signal obtained on an oscilloscop screen after amplification of the signal while compensating the RF pick up is shown in fig.2.2.

2.1.2 Low current probe

This probe consists of a small NE 102 A plastic scintillator which is coupled to a photo-multiplier via a light guide of 186 cm length. A cross section of the construction is shown in fig. 2.3 . The scintillator has an aluminium housing of 0.1 mm wall thickness and may be used at deuteron energies above 5 MeV. It may be used at currents between 0.1 and 50 nA. A typical signal from this probe is shown in fig. 2.4. No deterioration of the scintillator after use for several hours has been detected.

2.2 Measurements and results

Fig. 2.5 shows a block diagram of the electronics used for the measurements. By use of a time-to-amplitude converter (TAC) the mean phase can be determined to an accuracy of approximately 100 psec which corresponds to an accuracy in phase of 1.2^{o} at the 33 MHz RF frequency of the Karlsruhe Isochronous Cyclotron. The accuracy is limited by the width of the pulse height distribution behind the TAC. The spread of this distribution is due to a spread in pulse height of the primary pulses. So the accuracy could possibly be improved by replacing the discriminator for the pulses from the target by a differential discriminator or a fast zero crossing discriminator. A typical result of a phase versus radius measurement is shown in fig.2.6.

Using a special electronic system these probes have also been used to measure the pulse height distribution of single microstructure pulses.

3. Measurement of the phase width of the internal beam

The phase width of the internal beam determines the length of the microstructure pulses. It therefore limits the energy resolution of neutron time of flight measurements. It is thus very important to have fast and reliable methods of measuring the phase width and its dependence on machine parameters.

The phase width of the internal beam of the Karlsruhe Isochronous Cyclotron has been measured by Dietrich[2] using the method of Garren and Smith[3]. Similar measurements are described in section 3.1, and some limitations of the method are discussed. A second method which offers some advantages is described in section 3.2 .

3.1 Measurements by the method of Garren and Smith

3.1.1 Description of the method

When the accelerating frequency or the mean magnetic field (at all radii) is detuned by a certain amount the particles suffer a constant phase slip per revolution. For a sufficiently strong detuning the particles reach a phase $\pm \pi/2$ with respect to the maximum of the accelerating voltage, are then decelerated by the RF, and start moving back towards the machine center. The maximum radius reached by the particles depends on the starting phase, and so the distribution of maximum radii reflects the distribution in phase of the particles.
The phase $\phi(r)$ of a particle at radius r is connected to the starting phase ϕ_o by the equation

$$\sin \phi(r) = \sin \phi_o + 2\pi \frac{m\omega}{\Delta E} \int_o^r (\nu\omega - \omega_D)\, r dr \qquad (3.1)$$

m	particle mass
ΔE	energy gain per turn
ω	orbit angular frequency
ω_D	angular frequency of accelerating RF
ν	harmonic number (ratio of RF to orbit frequencies)

A derivation of this formula has, e.g., been given by Richardson (ref. 4, p. 70 f.) in a slightly different notation. Dietrich[2] has pointed out that equ. (3.1) is modified if the radial decrease of the accelerating voltage and the increase of the particle mass are taken into account.

In the measurements to be reportet the magnetic field was kept fixed and the accelerating frequency was detuned. Therefore we put

$$\omega = \frac{e}{m} (B_o + \Delta B) = \omega_o + \frac{e}{m} \Delta B$$

$$\omega_D = \nu\omega_o + \Delta\omega$$

e particle charge

Here ΔB represents an error in the mean magnetic field. ΔB may depend on the radius.

Inserting these expressions into equ. (3.1) and neglecting second order quantities we obtain

$$\sin \phi(r, \Delta\omega) = \sin \phi_o + 2\pi \frac{m\omega_o}{\Delta E} \int_o^r (\frac{e\nu}{m} \Delta B - \Delta\omega)\, r dr \qquad (3.2)$$

As $\sin \phi(r_m, \Delta\omega) = \pm 1$ at maximum radius r_m this leads to

$$\sin \phi_o = \pm 1 + 2\pi \frac{m\omega_D}{\Delta E} \left[\frac{\Delta\omega}{\nu} \frac{r_m^2}{2} - \frac{e}{m} \int_o^{r_m} \Delta B(r)\, r dr \right] \qquad (3.3)$$

Combining eq. (3.3) with equ. (3.2) for $\Delta\omega = 0$ we finally obtain

$$\sin \phi(r_m, o) = \pm 1 + \pi \frac{m\omega_D \Delta\omega}{\nu \Delta E} r_m^2 \qquad (3.4)$$

The left hand side of this equation represents the phase of a particle at the radius r_m when the accelerating frequency has the normal value. The right hand side can be determined by detuning the frequency by such an amount that the particle turns back at radius r_m . In equ. (3.4) the upper sign should be taken for negative values of $\Delta\omega$ and vice versa such that the two terms of the sum always have opposite signs.

We now consider a starting phase ϕ_p defined by the condition that the fraction of particles with $\phi > \phi_p$ is p. For $\Delta\omega < o$ all particles with $\phi > \phi_p$ will start moving back towards the machine center at radii smaller than the maximum radius corresponding to ϕ_p, as can be seen from equ. (3.2). The maximum radius of a particle with $\phi = \phi_p$ is therefore that point at which the current has dropped to the fraction p of its value near machine center. This point can easily be measured for different values of $\Delta\omega$ and p, and by use of eq. (3.4) the phase history of the whole beam can be determined.

It should be mentioned that the starting conditions of the beam may be changed by a strong detuning of the radio frequency, which by virtue of eq. (3.4.) limits the range of radii at which the phase distribution of the beam may be measured by this method.

1.2 Measurements and results

Fig. 3.1 shows a set of measurements of current versus radius for different deviations of the radio frequency from the normal value. Fig. 3.2 gives the phase history of particles with $\phi = \phi_p$ for p = 0.1, 0.2 ... 0.9. Considerable differences exist

between the results obtained from positive and negative frequency shifts, respectively. From Fig. 3.2 integral and differential distributions of particles versus phase at a fixed radius can easily be derived. The results are shown in Fig. 3.3 . In spite of the above mentioned discrepancies the phase widths obtained from positive and negative frequency shifts are in good agreement.

Figs. 3.4 to 3.6 show the same results for a setting of the machine which differs from the first one only in that the RF amplitude was reduced by 5 %. Due to the slits defining the beam near the machine center the phase width of the beam is reduced by approximately 30 %. This difference in phase width is also reflected in the radial beam densities which are shown in Fig. 3.7 and 3.8 for the two RF amplitudes, respectively.

3.1.3 Limitations of the method

The main objection which must be put forward against the theoretical considerations of section 3.1.1 is the complete disregard of radial oscillations. When radial oscillations are present the maximum radius measured is not the quantity r_m of equs (3.3) and (3.4), but $r_m + a$ where a is the instantaneous value of the coherent radial oscillation. It has therefore been pointed out by Blosser[5] that the method is only applicable when the beam is well centered. Further complication arises when a first harmonic is present in the magnetic field. As is well known a first harmonic will excite coherent radial oscillations the amplitude of which is an oscillating function of the energy gain per turn[6]. As the energy gain per turn at a fixed radius is changed by detuning the frequency due to the phase slip the amplitude of the radial oscillations is expected to depend on the amount of detuning. While the last mentioned difficulty can be avoided by a careful tuning of the machine the following limitations of the method are inherent:

a) It is only applicable to the internal beam, and it is by no means certain that the phase width is unchanged by extraction.

b) One set of phase width measurements takes about one hour, so the method can hardly be used for routine checking of the accelerator.

Therefore a second method was developed which avoids the above mentioned drawbacks.

3.2 Measurements of the time distribution of prompt γ rays

3.2.1 Description of the method

The method to be described was first used by H. Brückmann and E. Haase[7] on the external cyclotron beam. The principle procedure is described in fig. 3.9 . The internal beam is stopped by a solid target in which (among other radiations) prompt γ rays are produced. These γ rays are detected by a scintillation counter placed approximately 5 m from the cyclotron. Only the largest pulses from the scintillation counter are accepted to trigger a fast discriminator the output of which starts a time-to-amplitude converter (TAC). The TAC is stopped by a signal derived from the cyclotron RF which is coupled from the tank or the RF generator. When the stop signal appears at fixed phase of the cyclotron RF the time distribution of the γ rays reflects the intensity distribution of the particles versus phase. The following precautions should be taken:

a) The frequency of the γ pulses used to start the TAC should be considerable smaller than the RF frequency such that the probability that two γ rays above threshold are accepted during the same microstructure pulse is negligible.

b) To avoid systematic errors due to delayed γ rays excited by the beam only the most energetic γ rays should be accepted.

3.2.2 Details of the procedure

As can be seen from figs 3.3 and 3.6 the width of the time distribution to be expected is approximately 1 nsec. Therefore a good timing of the γ ray pulse is necessary. The timing properties of scintillation counters have been studied extensively in connection with nuclear spectroscopy investigations[8]. Our set-up differs from these measurements in the following respects:

a) The time jitter of the scintillator-photomultiplier system occurs only in one of the coincidence channels whereas in the other one the jitter is negligible.
b) γ rays of very high energy (up to 10 MeV) are available among the prompt radiation.
c) The measurements can be confined to a small range of γ ray energies.

Under these circumstances the leading edge timing method has the smallest jitter induced by phosphor decay statistics and transit time fluctuations[9].

As no γ rays of comparable energy are available from radioactive sources the time resolution of the system was tested in an arrangement shown in fig. 3.10. Two photomultipliers looking at the same plastic scintillator provide the start and stop pulses for the TAC. The low-level discriminator delivers an output pulse starting at that moment when the input pulse crosses the threshold. For leading edge timing the threshold for the lower level discriminators are set at very low values. In order to suppress small pulses the lower level discriminator is gated by the output of a second discriminator with the threshold set at a very high value (upper level discriminator). The result of a measurement using a magnesium target and 30 MeV deuterons is shown in fig. 3.11 .

The threshold of the upper level discriminators was chosen to give an input rate of 3 kHz at the TAC. The different slopes of the two sides of the intensity distribution indicate a difference in the time resolution of the two multipliers. For comparison we show in fig. 3.12 the resolution obtained with the same electronic system and photomultipliers using two different plastic scintillators and a ^{60}Co source.

Tests of the time jitter of the electronic system as well as of the signals derived from the RF gave results below 50 psec. We therefore assume that the time resolution of our phase measurement system using the better of the two photomultipliers is better than $330/\sqrt{2} \approx 240$ psec.

3.2.3 Measurements and results

The target material used should be chosen according to the following requirements:

a) No γ emitting isomer of a half-life between 0.1 and 10 nsec should be excited.
b) The ratio of γ rays to neutrons emitted from the target should be as high as possible.

As the γ rays were measured under approximately 120° with respect to the beam direction only evaporation neutrons are expected to arrive at the scintillator. Due to the flight path of more than 5 m and the continuous energy spectrum of evaporation neutrons these neutrons form a constant background in the time distribution. Fig. 3.13 shows a time distribution as displayed on the screen of the pulse height analyzer.

Fig. 3.14 shows the result of a phase width measurement using different target materials. The neutron background has been subtracted. Within the accuracy of measurement the half widths of the distributions are identical, so no influence of isomers was found (as might have been suspected for γ rays of so high an energy). The ratio of γ rays to neutrons was highest for the magnesium target. At a current of 1 µA the time for

one measurement is approximately 3 min. The method was applied for deuteron and α particle energies above 10 MeV.

3.2.4 Conclusion

In our opinion the advantage of the procedure described in this section is that it provides detailed and accurate information on the phase width of the internal or external beam in a few minutes and without recourse to extensive calculations and theories. It therefore offers the possibility to see immediately the influence of any parameter change on the phase width.

4. Measurement of the phase space volume of the external cyclotron beam

One of the important figures characterising the quality of a beam of particles is the volume in phase space occupied by the particles as, according to Liouville's Theorem, this figure is not changed by the elements of the beam handling system. Let us introduce a Cartesian coordinate system x, y, z, such that z is the direction of propagation of the beam, x denotes the horizontal and y the vertical coordinate, respectively. The beam handling system usually consists of deflecting magnets bending the beam in a horizontal plane, and magnetic quadrupol lenses focusing or defocusing the beam horizontally or vertically. Then the motion of particles in the three coordinates x, y, and z is completely decoupled in the linear approximation, and Liouville's Theorem does not only hold in the six-dimensional phase space (x,y,z,p_x,p_y,p_z), but also in each of the three subspaces (x,p_x), (y,p_y), and (z,p_z) separately.

This section describes measurements of the phase space occupied by the beam in the (x,p_x)- and (y,p_y)-planes. Instead of p_x and p_y we use the variables $x' = p_x/p_o$ and $y' = p_y/p_o$, respectively, where p_o is the mean momentum of the particles.

4.1 Principle of the procedure

The width of the beam at a fixed distance behind a quadrupole lens depends on the excitation of the lens. When the excitation of a focusing single quadrupole is increased from zero the width will decrease, pass through a minimum and start to increase again. The minimum is obtained when the focus of the beam behind the quadrupole is situated at the position of measurement. The rate of increase of the width at either side of the minimum is dependent on the divergence of the beam at the focus. It is therefore evident that the measurement of the width at different excitations will yield information on the width and divergence of the beam at the focus and thus on the phase space of the beam.

If the particle density of the beam is assumed to be a two-dimensional Gaussian function of x and x', e.g., it can be shown that the square of the full width at half maximum H of the beam at a fixed distance from the quadrupole is a second order function of the inverse of the focal length f of the lens:

$$H^2 = C\left[\frac{S_2}{f} - A\right]^2 + B \qquad (1)$$

Here s_2 is the distance from the center of the quadrupole to the point of measurement, and A,B, and C are parameters characterizing the second order function. The phase space volume occupied by a fraction q of the beam is related to these parameters by

$$Q = \frac{-\pi}{4\ln 2}\,\frac{\sqrt{BC}}{s_2}\,\ln(1-q) \qquad (2)$$

The proof of formulae (1) and (2) is given in the appendix.

4.2 Measurements and results

The width of the beam was measured with a rotating wire of 0.5 mm thickness.
The focal length of the single quadrupole lenses was taken from tables supplied by the manufacturer[+]. These tables also give the position of the principal planes. As these never deviated by more than 0,7 cm from the center of the lens the thin lens approximation used in the appendix was sufficiently accurate.

Measurements were carried out at two different positions M 1 and M 2 along the beam pipes the lay-out of which is shown in fig. 4.1 . The quadrupole lenses Q 1, Q 2, Q 9, and Q 11 were used. The current flowing to the rotating wire was registered with a recorder. The total beam currents amounted to several μA.

Fig. 4.2 shows the result of a series of measurements for different excitations of one of the quadrupole lenses. As can be seen, the data are fitted by a parabola to sufficient accuracy.

The results of the measurements are given in tables 1 and 2 for the horizontal and vertical phase space, respectively. While the agreement of the independent measurements is satisfactory for the horzizontal phase space, the results of vertical phase space measurements scatter considerably. As the figures obtained at position M 2 (see fig. 4.1) are consistently lower than those obtained at M 1, it is suspected that part of the beam was lost in the switching magnet which has a gap height of 6 cm. This would be expected to reduce the vertical phase space and to leave the horizontal phase space unaltered. Unfortunately , the transmission of the switching magnet was not

---

[+] Allgemeine Elektricitätsgesellschaft, Fachbereich Beschleunigungsanlagen, Frankfurt/Main

checked. We therefore consider the following numbers the correct results:

$$Q_H \ (50\ \%) = 5.6\,[\text{mm . mrad}]$$
$$Q_V \ (50\ \%) = 8.7\,[\text{mm . mrad}]$$

Table 1

Results of the measurements of horizontal phase space . Symbols are defined in fig. 4.1 and in the appendix

No	Position	Lens	Distance s_2 [cm]	Distance s_1 [cm]	Phase space Q(50 %)mm mrad
1	M 1	Q 9	155.5	203.5	5.39
2			161.5	205.8	5.61
3	M 1	Q 11	75.5	243.6	5.79
4			81.5	253.7	5.78
5	M 2	Q 1	170.5	196.2	5.07
6			176.5	187.1	5.61
7	M 2	Q 2	137.5	223.6	5.66
8			143.5	208.8	5.72
		mean value			5.58 ± 0.085

Table 2

Results of the measurements of vertical phase space.

Symbols are defined in fig. 4.1 and in the appendix.

No	Position	Lens	Distance s_2 [cm]	Distance s_1 [cm]	Phase space Q(50 %) [mm mrad]
9	M 1	Q 9	155.5	143.6	8.82
10			161.5	124.1	8.43
11	M 1	Q 11	75.5	188.8	8.82
12			81.5	189.5	8.88
13	M 2	Q 1	170.5	81.1	3.93
14			176.5	76.3	5.27
15	M 2	Q 2	137.5	104.6	4.90
16			143.5	103.7	6.37
			mean value of measurements 9-12		8.74 ± 0.104

5. Acknowledgements

We are indebted to Miss Chr. Rämer for her assistance in taking and analyzing the data. The important contributions of H. Bellemann to the construction of the targets, and of G. Bauer and H. Müller to setting-up and preparing the measurements are gratefully acknowledged. Thanks are also due to the operating staff under F. Schulz for their efficient cooperation.

References:

1) H.H. Feldmann, Thesis, Technische Universität Berlin (1964); IEEE Transactions Nucl. Sc. NS-13, 30 (August 1966)

2) H. Dietrich, IEEE Transactions Nucl. Sc. NS-13, 36 (August 1966)

3) A.A. Garren and L. Smith, CERN 63-19, p. 18 (1963)

4) J.R. Richardson, Progress Nucl. Techn. Instrumentation 1, 1 (1965)

5) H.G. Blosser, IEEE Transactions Nucl. Sc. NS-13, 1 (August 1966)

6) J. D. Lawson, Nucl. Instr. Meth. 49, 114 (1967)

7) H. Brückmann, and E. Haase, private communication

8) A. Schwarzschild, Nucl. Instr. Meth. 21, 1 (1963); G. Bertolini, M. Cocchi, V. Mandl, and A. Rota, IEEE Transactions Nucl. Sc. NS-13, 119 (June 1966); E. Gatti and V. Svelto, Nucl. Instr. Meth. 43,248 (1966); and references cited therein.

9) R.E. Bell, Nucl. Instr. Meth. 42, 211 (1966)

Appendix

The particle density in two-dimensional phase space is assumed to be a two-dimensional Gaussian function

$$F(x,x') = N \exp\left\{-\frac{1}{2}\left(m_{11}x^2 + 2m_{12}xx' + m_{22}x'^2\right)\right\} \qquad (A\ 1)$$

where N is a normalizing factor

$$N = \frac{1}{2\pi}\sqrt{D}\,; \qquad D = m_{11}\,m_{22} - m_{12}^2 \qquad (A\ 2)$$

The spatial distribution of the particles can be obtained from F(x,x') by integrating with respect to x' :

$$F_s(x) = \int_{-\infty}^{+\infty} F(x,x')\,dx' = \frac{1}{\sqrt{2\pi}\Sigma}\exp\left\{-\frac{1}{2}\frac{x^2}{\Sigma^2}\right\} \qquad (A\ 3)$$

where

$$\Sigma^2 = \frac{m_{22}}{D}\,. \qquad (A\ 4)$$

Now let (x_1, x_1') be the transverse displacement and direction corresponding to (x,x') at another point along the path of the particles. Then, in first approximation, (x_1, x_1') are connected with (x,x') by a transformation matrix T.

$$\begin{bmatrix} x \\ x' \end{bmatrix} = \begin{bmatrix} t_{11} & t_{12} \\ t_{21} & t_{22} \end{bmatrix} \cdot \begin{bmatrix} x_1 \\ x_1' \end{bmatrix}$$

Denoting the points corresponding to (x,x') and (x_1,x_1') P and P_1, respectively, the phase space density at P_1 can be obtained from the density at P simply by putting

$$F_1(x_1, x_1') = F\left[x(x_1, x_1'), x'(x_1, x_1')\right]$$

because the determinant of T equals unity as a direct consequence of Liouville's Theorem. For a drift space of length s

between P and P_1 the matrix T is given by

$$T = \begin{bmatrix} 1 & -s \\ 0 & 1 \end{bmatrix}$$

It is then a trivial but tedious task to evaluate the spatial width of the beam at P_1 represented by Σ:

$$\Sigma^2(s) = \frac{1}{D}(m_{11}s^2 - 2m_{12}s + m_{22}) \qquad (A\ 5)$$

As can be seen from (A 4) and (A 2), $m_{11} > 0$. Therefore $\Sigma^2(s)$ attains a minimum at $s = \frac{m_{12}}{m_{11}}$. At this point the phase space density can be written

$$F_m(x_m, x'_m) = \frac{1}{2\pi\sigma\sigma'} \exp\left\{-\frac{1}{2}\left(\frac{x_m^2}{\sigma^2} + \frac{x'^2_m}{\sigma'^2}\right)\right\} \qquad (A\ 6)$$

where

$$\sigma^2 = \frac{1}{m_{11}} \quad \text{and} \quad \sigma'^2 = \frac{m_{11}}{D}\ .$$

This means that at a point of minimum diameter of a beam the distributionsof particles with respect to space and direction are independent.

For the experimental set-up in fig. 4.1 we will approximate the effect of the quadrupole by the thin lens formula and assume that at a distance s_1 before the quadrupole the phase space density has the form of equ. (A 6). The distance between quadrupole and rotating wire is denoted by s_2. The linear transformation between (x_1, x'_1) and (x_2, x'_2) is then given by

$$\begin{bmatrix} x_2 \\ x'_2 \end{bmatrix} = \begin{bmatrix} 1 & s_2 \\ 0 & 1 \end{bmatrix} \begin{bmatrix} 1 & 0 \\ -\frac{1}{f} & 1 \end{bmatrix} \begin{bmatrix} 1 & s_1 \\ 0 & 1 \end{bmatrix} \begin{bmatrix} x_1 \\ x'_1 \end{bmatrix} = T^{-1} \begin{bmatrix} x_1 \\ x'_1 \end{bmatrix}$$

It is again easy in principle to evaluate the width of the beam at P_2:

$$\Sigma^2 = (\sigma^2 + s_1^2\,\sigma'^2)\left[\frac{s_2}{f} - \frac{\sigma^2 + (s_1 + s_2)s_1\sigma'^2}{\sigma^2 + s_1^2\sigma'^2}\right]^2 + \frac{\sigma^2\sigma'^2 s_2^2}{\sigma^2 + \sigma'^2 s_1^2}$$

$$\equiv c\left[\frac{s_2}{f} - a\right]^2 + b \qquad \text{(A 7)}$$

It then follows

$$\sigma^2\sigma'^2 = \frac{b \cdot c}{s_2^2} ;$$

The quantity easily measured is the total width at half maximum $H = \sqrt{8\ln 2}\ \Sigma$ of the spatial distribution. If the measured points for different values of f are approximated by a parabola

$$H^2 = C\left[\frac{s_2}{f} - A\right]^2 + B \qquad \text{(A 8)}$$

it follows

$$\sigma' = \frac{1}{s_2}\sqrt{\frac{B + C(A-1)^2}{8\ln 2}}\,;\ \sigma = \sqrt{\frac{1}{8\ln 2}\,\frac{BC}{B+C(A-1)^2}} \qquad \text{(A 9)}$$

$$\sigma\sigma' = \frac{1}{s_2}\,\frac{\sqrt{BC}}{8\ln 2}\,;\ s_1 = \frac{C(A-1)s_2}{B+C(A-1)^2}$$

A more reasonable figure to quote as beam quality is the minimum area in phase space that contains a given fraction q of the beam intensity. This is most easily calculated at the point P_1 where this area is an ellipse with half-axes $a\sigma$ and $a\sigma'$

$$Q = \pi a^2 \sigma\sigma'$$

The quantity a is determined by the equation

$$\frac{1}{2\pi\sigma\sigma'} \iint \exp\left\{-\frac{1}{2}\left(\frac{x^2}{\sigma^2} + \frac{x'^2}{\sigma'^2}\right)\right\} dxdx' = q$$

where the domain of integration is the interior of the ellipse defined by

$$\frac{x^2}{\sigma^2} + \frac{x'^2}{\sigma'^2} = a^2$$

This can be solved to yield

$$a^2 = -2 \ln (1 - q)$$

$$Q = -2\pi\sigma\sigma' \ln (1 - q)$$

Introducing the measured quantities B and C defined above we obtain

$$Q = -\frac{2\pi}{s_2} \frac{\sqrt{BC}}{8\ln 2} \ln (1 - q) = -\frac{1.13}{s_2} \sqrt{BC} \ln (1 - q) \qquad (A\,10)$$

$$Q(50\%) = \frac{\pi}{4} \frac{\sqrt{BC}}{s_2} = \frac{0.785}{s_2} \sqrt{BC}$$

Figure captions

Fig. 2.1 View of high current probe.

Fig. 2.2 A typical signal from high current probe. Mean beam current 10 μA. Abscissa 2 ns/div.. Ordinate 100 mV/div.

Fig. 2.3 Cross section of low current probe.

Fig. 2.4 A typical signal from low current probe Mean beam current 1 nA. Abscissa 5 nsec/div.. Ordinate 20 mV/div.

Fig. 2.5 Block diagramof phase measurement experiment

Fig. 2.6 Dependence of phase on radius for slightly detuned trim coils.

Fig. 3.1 Measured deuteron currents versus radius for different frequency shifts at normal RF amplitude.

Fig. 3.2 Phase distribution of a deuteron beam versus radius for normal RF amplitude as derived from fig. 3.1 .

Fig. 3.3 Phase distribution of the beam at fixed radius for normal RF amplitude as derived from fig. 3.2.

Fig. 3.4 Measured deuteron currents versus radius for different frequency shifts at lower RF amplitude

Fig. 3.5 Phase distribution of a deuteron beam versus radius for lower RF amplitude as derived from fig. 3.4.

Fig. 3.6 Phase distribution of the beam at fixed radius for lower RF amplitude as derived from fig. 3.5.

Fig. 3.7 Radial beam density at $\Delta f = 0$ for the machine setting of figs. 3.1 to 3.3. Numbers below trace indicate the radius in mm. Measurement was made with a Siemens Oszillomink recorder of 800 Hz nominal band width.

Fig. 3.8 Radial beam density at $\Delta f = 0$ for the machine setting of figs. 3.4 to 3.6.

Fig. 3.9 Principle of phase distribution measurement by time distribution of prompt γ rays.

Fig. 3.10 Arrangement for testing the time resolution of the system.

Fig. 3.11 Result of time resolution measurement using a 30 MeV deuteron beam and a Mg target.

Fig. 3.12 Time resolution of the system for ^{60}Co γ rays.

Fig. 3.13 Measured time distribution of prompt γ rays as displayed by the multichannel analyser. The continuous neutron background is to be seen clearly. The target was Mg, beam current 1 μA, and deuteron energy 25 MeV. Horizontal scale is 45 psec per channel.

Fig. 3.14 Phase distribution of the beam as measured with different target materials. The neutron background has been subtracted.

Fig. 4.1 Lay-out of the part of the beam handling system used for the phase space measurements.

M1, M2 : Position of measurements; Q1, Q2, Q9, Q10,Q11: quadrupole magnets.

Fig. 4.2a Results of one of the phase space measurements. The square of the FWHM H is plotted versus the reciprocal of the focal length f.

Fig. 4.2b Part of fig. 4.2a close to the minimum.

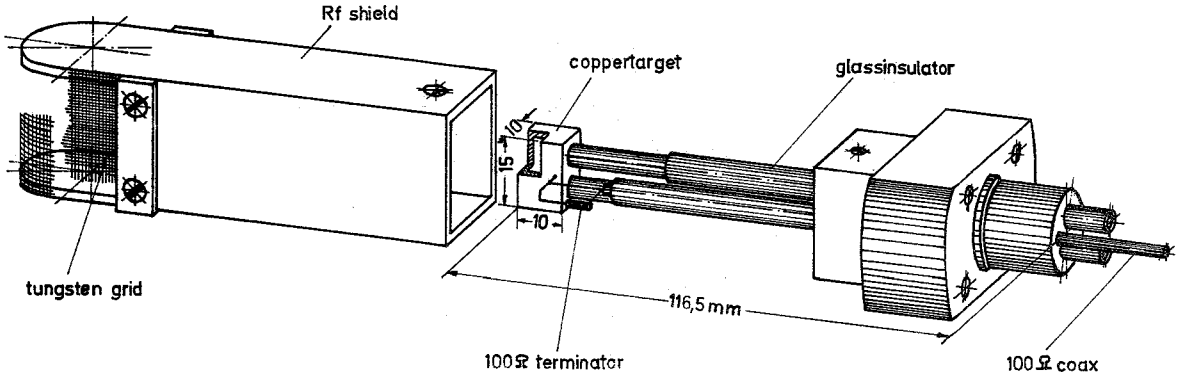
Rf shield
coppertarget
glassinsulator
10
15
10
tungsten grid
116,5 mm
100Ω terminator
100Ω coax

Fig. 2.1

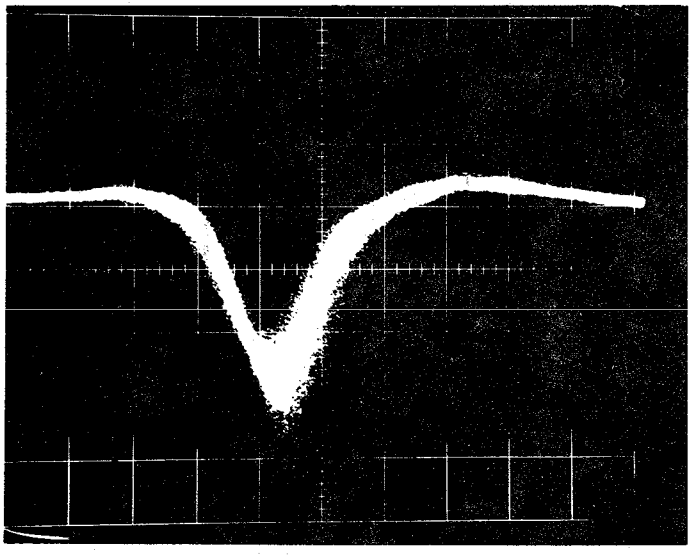

Fig. 2.2

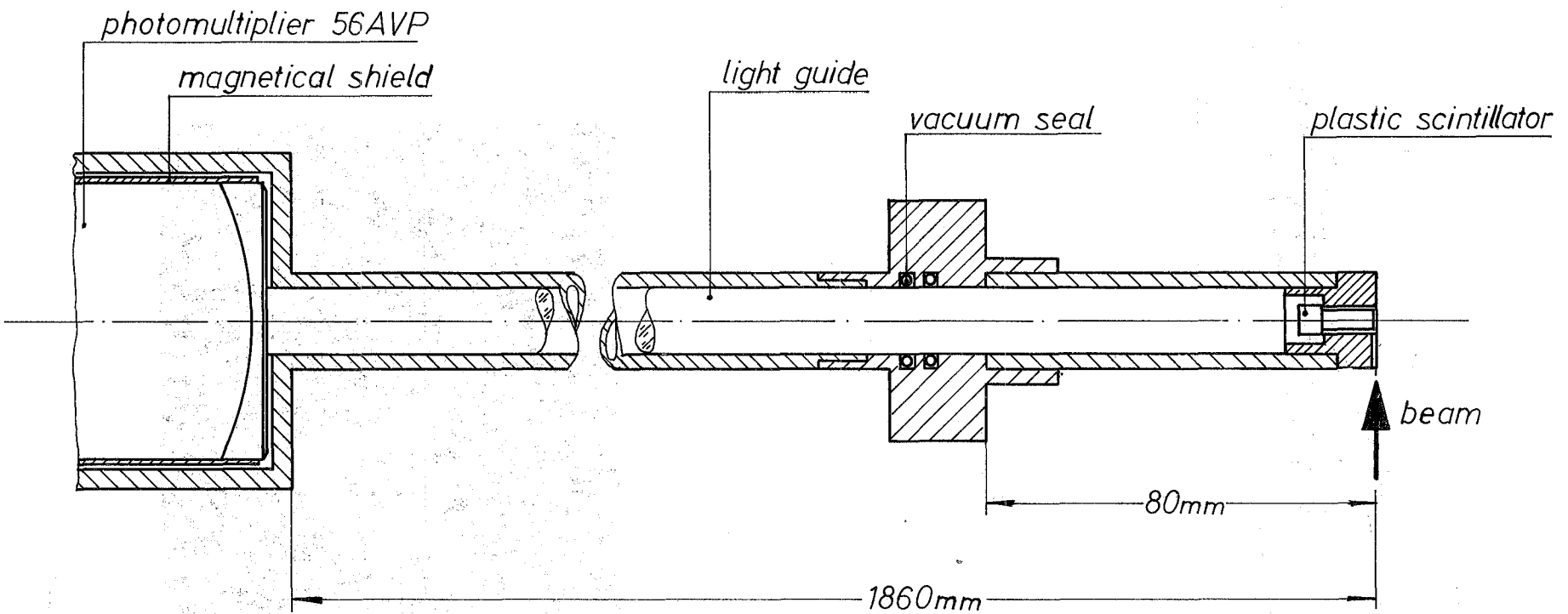
photomultiplier 56AVP
magnetical shield
light guide
vacuum seal
plastic scintillator
beam
80mm
1860mm

Fig. 2.3

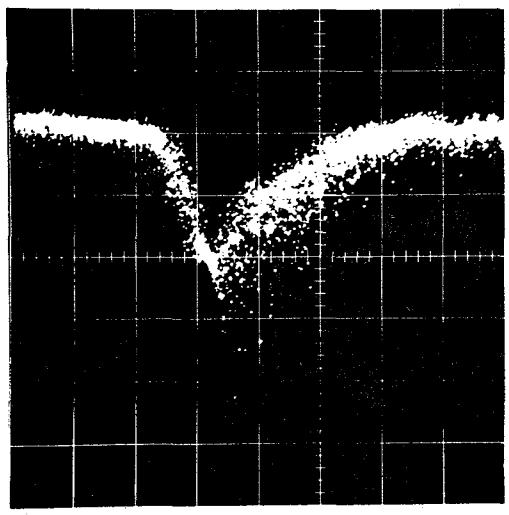

Fig. 2.4

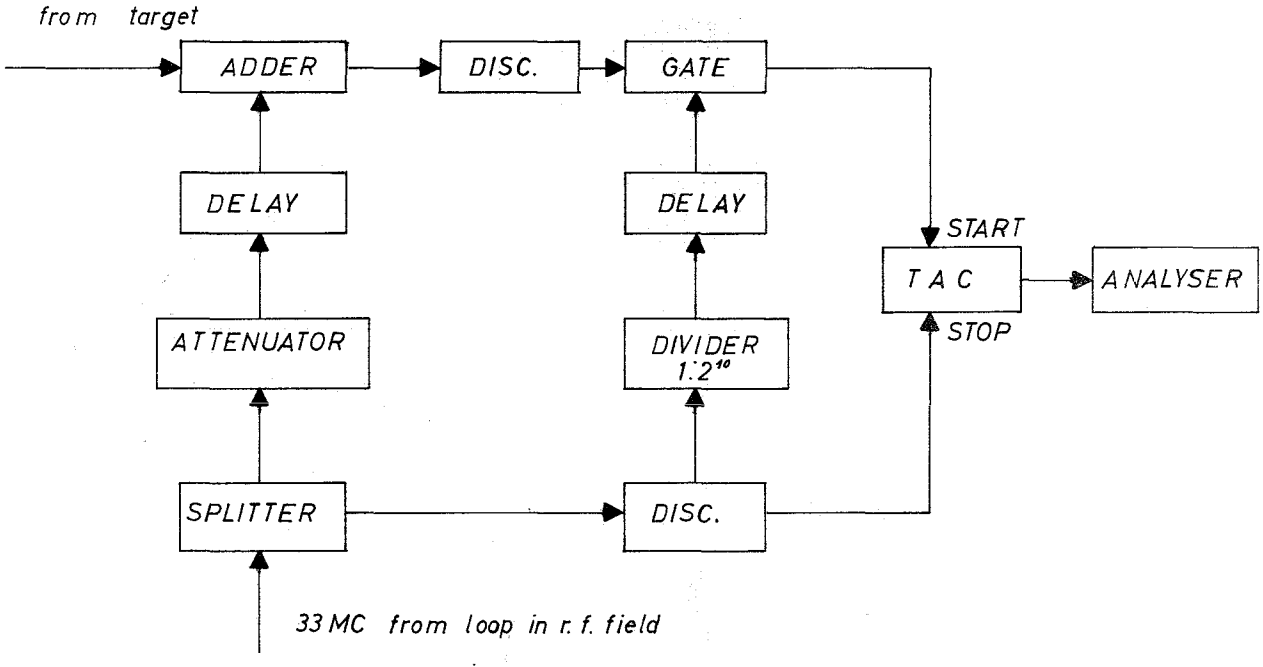
from target
ADDER
DISC.
GATE
DELAY
DELAY
START
T A C
ANALYSER
STOP
ATTENUATOR
DIVIDER
1:2^10
SPLITTER
DISC.
33 MC from loop in r. f. field

Fig. 2.5

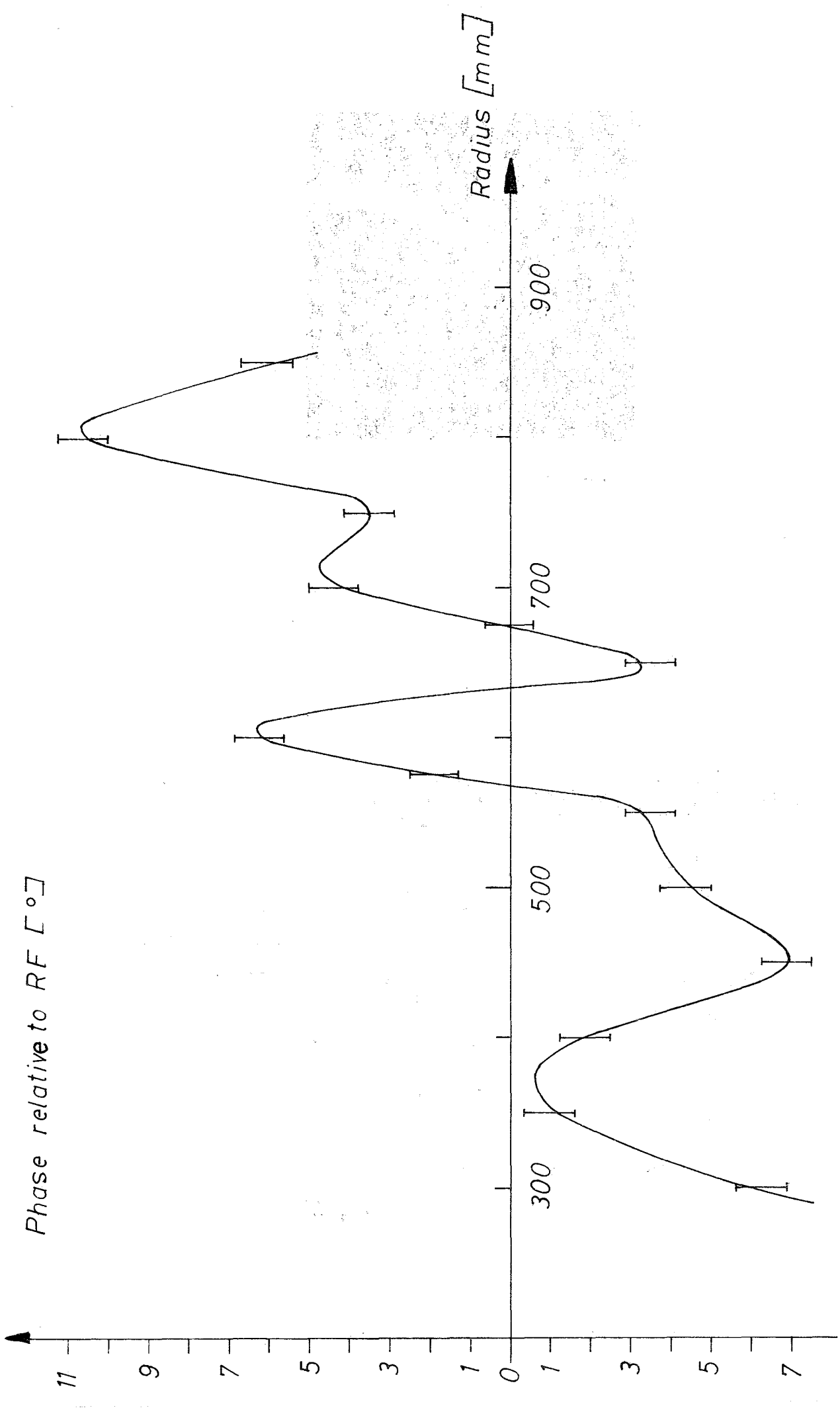

Fig. 2.6

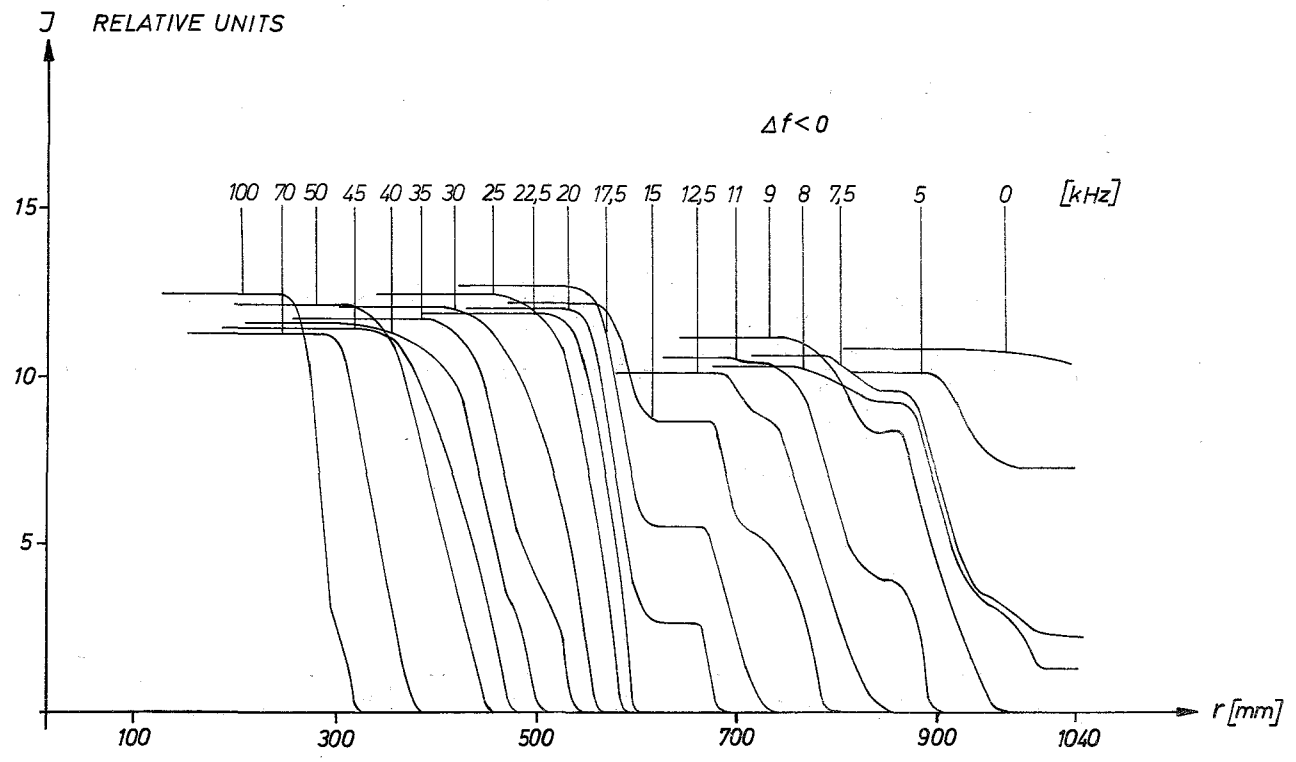
J RELATIVE UNITS
Δf<0
100 70 50 45 40 35 30 25 22,5 20 17,5 15 12,5 11 9 8 7,5 5 0 [kHz]
15
10
5
100
300
500
700
900
1040
r [mm]

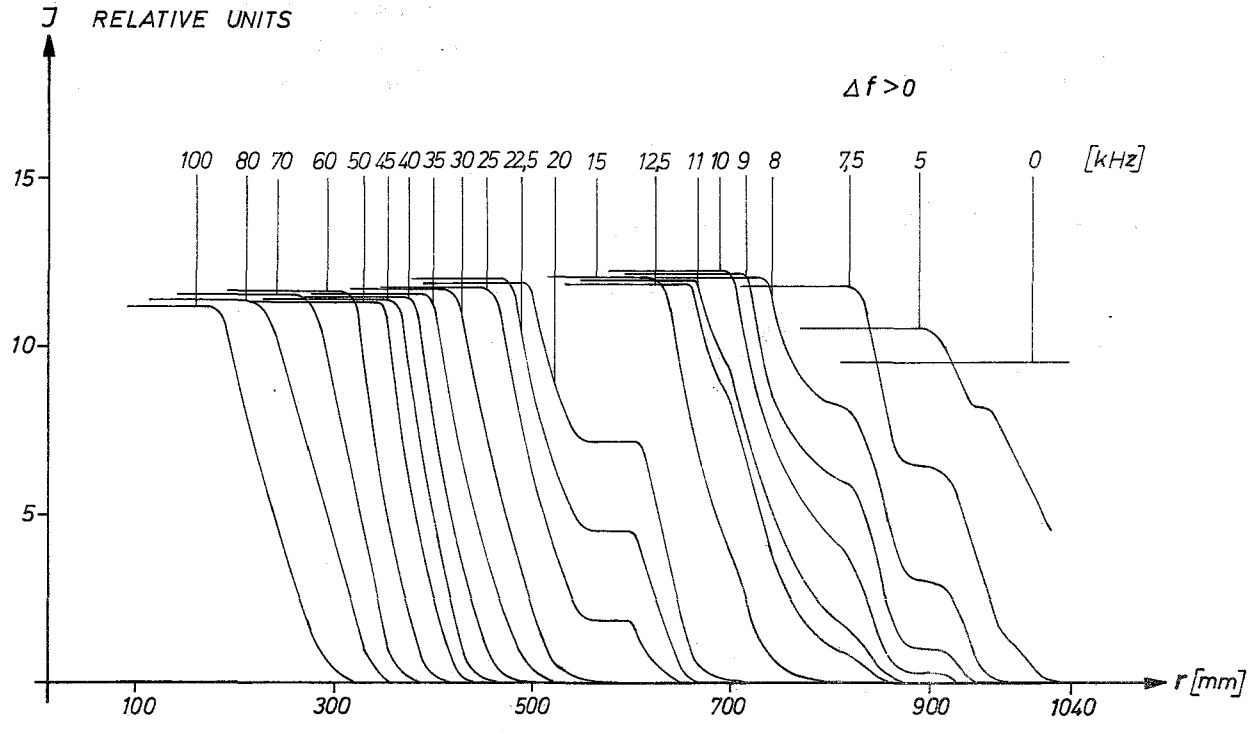
J RELATIVE UNITS
Δf>0
100 80 70 60 50 45 40 35 30 25 22,5 20 15 12,5 11 10 9 8 7,5 5 0 [kHz]
15
10
5
100
300
500
700
900
1040
r [mm]

Fig. 3.1

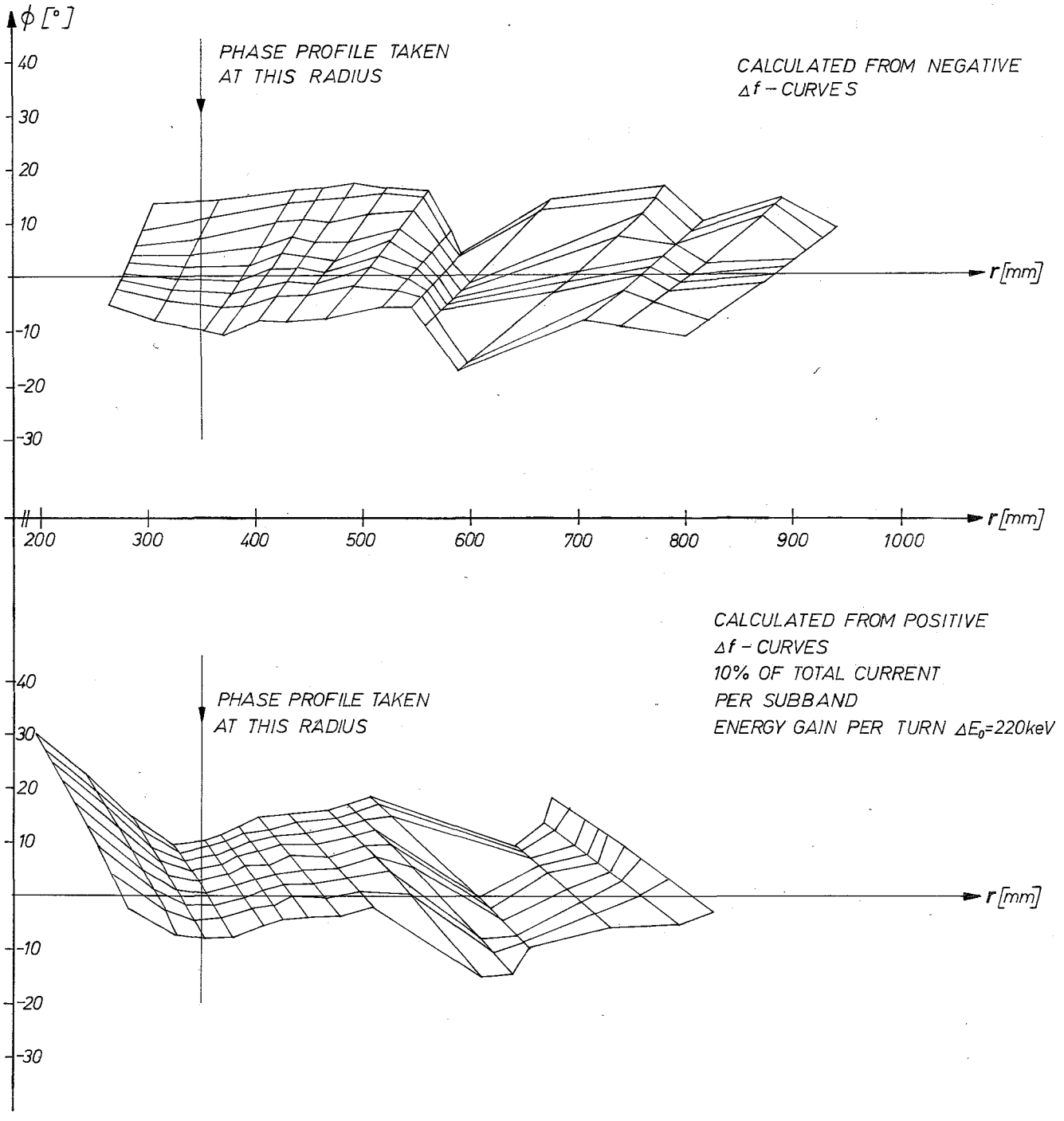
ϕ [°]
40
30
20
10
-10
-20
-30
PHASE PROFILE TAKEN
AT THIS RADIUS
CALCULATED FROM NEGATIVE
Δf – CURVES
r[mm]
200
300
400
500
600
700
800
900
1000
CALCULATED FROM POSITIVE
Δf – CURVES
10% OF TOTAL CURRENT
PER SUBBAND
ENERGY GAIN PER TURN ΔE0=220keV
PHASE PROFILE TAKEN
AT THIS RADIUS

Fig. 3.2

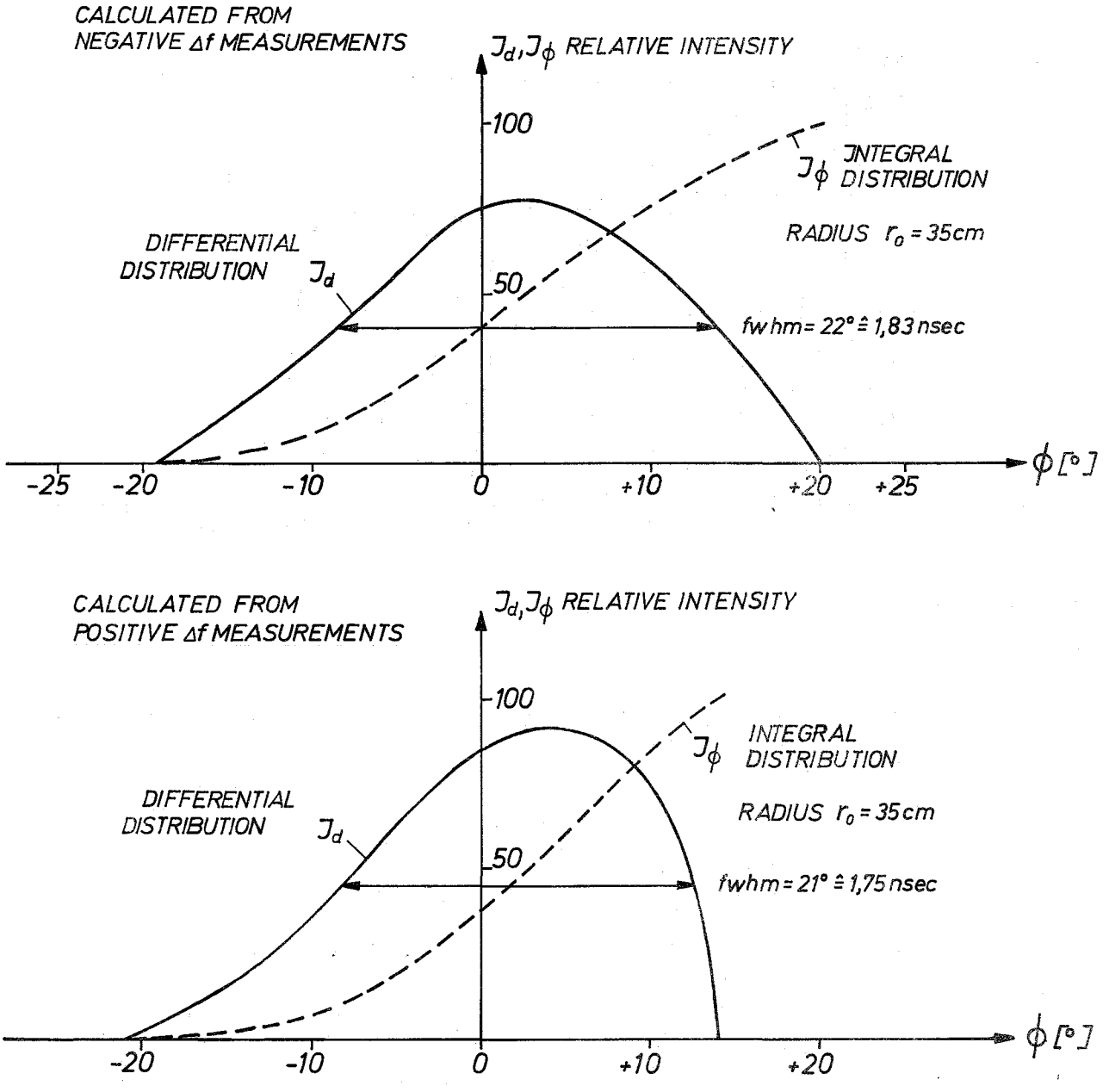
CALCULATED FROM
NEGATIVE Δf MEASUREMENTS
J_d, J_ϕ RELATIVE INTENSITY
100
J_ϕ INTEGRAL DISTRIBUTION
RADIUS $r_0 = 35cm$
DIFFERENTIAL DISTRIBUTION J_d
50
fwhm = 22° ≙ 1,83 nsec
-25 -20 -10 0 +10 +20 +25
ϕ [°]
CALCULATED FROM
POSITIVE Δf MEASUREMENTS
J_d, J_ϕ RELATIVE INTENSITY
100
J_ϕ INTEGRAL DISTRIBUTION
RADIUS $r_0 = 35cm$
DIFFERENTIAL DISTRIBUTION J_d
50
fwhm = 21° ≙ 1,75 nsec
-20 -10 0 +10 +20
ϕ [°]

Fig. 3.3

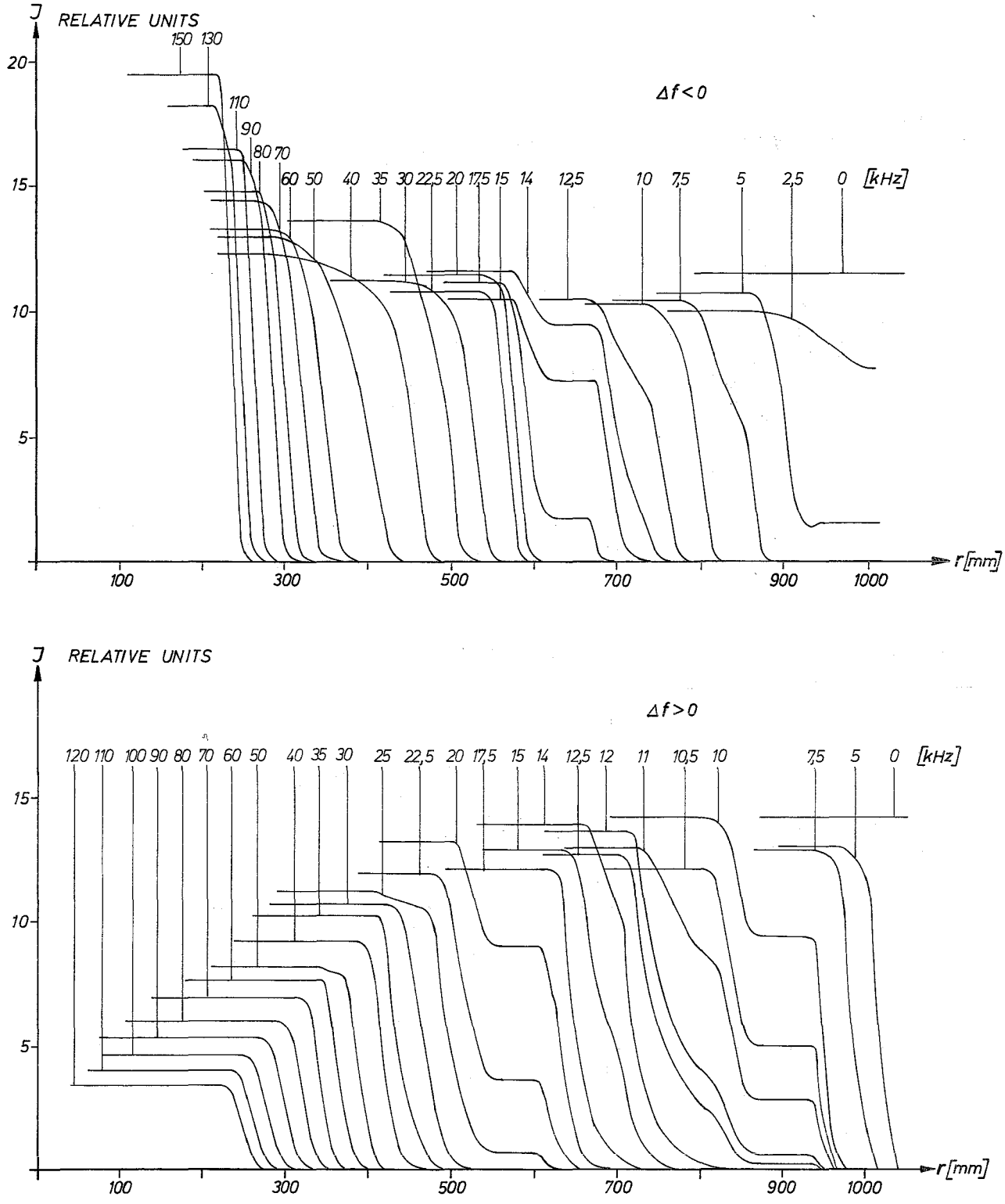
J RELATIVE UNITS
150 130
110
90
80 70
60 50 40 35 30 22,5 20 17,5 15 14 12,5 10 7,5 5 2,5 0 [kHz]
Δf < 0
20
15
10
5
100 300 500 700 900 1000
r[mm]
J RELATIVE UNITS
Δf > 0
120 110 100 90 80 70 60 50 40 35 30 25 22,5 20 17,5 15 14 12,5 12 11 10,5 10 7,5 5 0 [kHz]
15
10
5
100 300 500 700 900 1000
r[mm]

Fig. 3.4

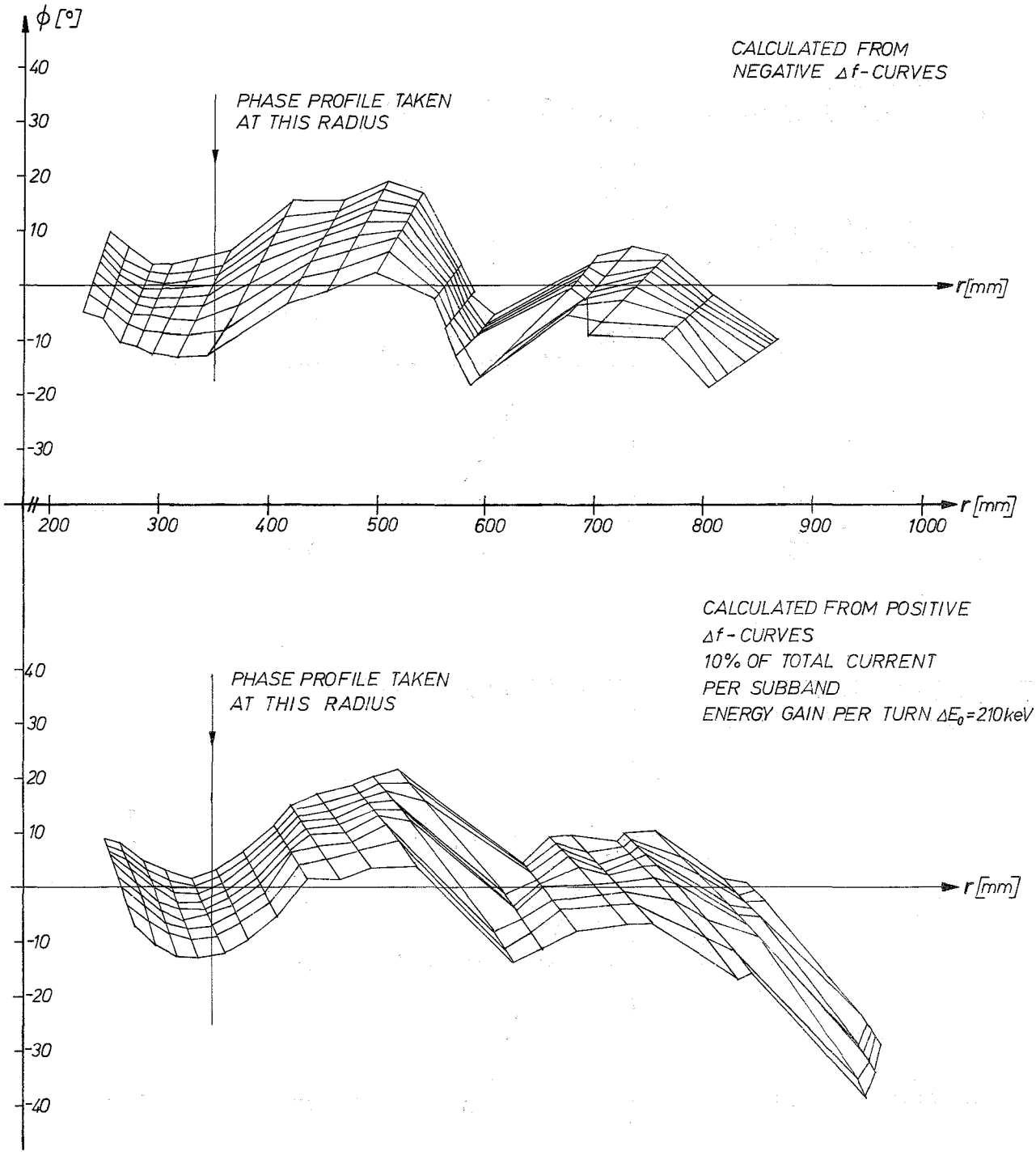
ϕ [°]
40
30
20
10
-10
-20
-30
CALCULATED FROM
NEGATIVE Δf-CURVES
PHASE PROFILE TAKEN
AT THIS RADIUS
r[mm]
200
300
400
500
600
700
800
900
1000
r [mm]
CALCULATED FROM POSITIVE
Δf-CURVES
10% OF TOTAL CURRENT
PER SUBBAND
ENERGY GAIN PER TURN ΔE0=210keV
PHASE PROFILE TAKEN
AT THIS RADIUS
40
30
20
10
-10
-20
-30
-40
r [mm]

Fig. 3.5

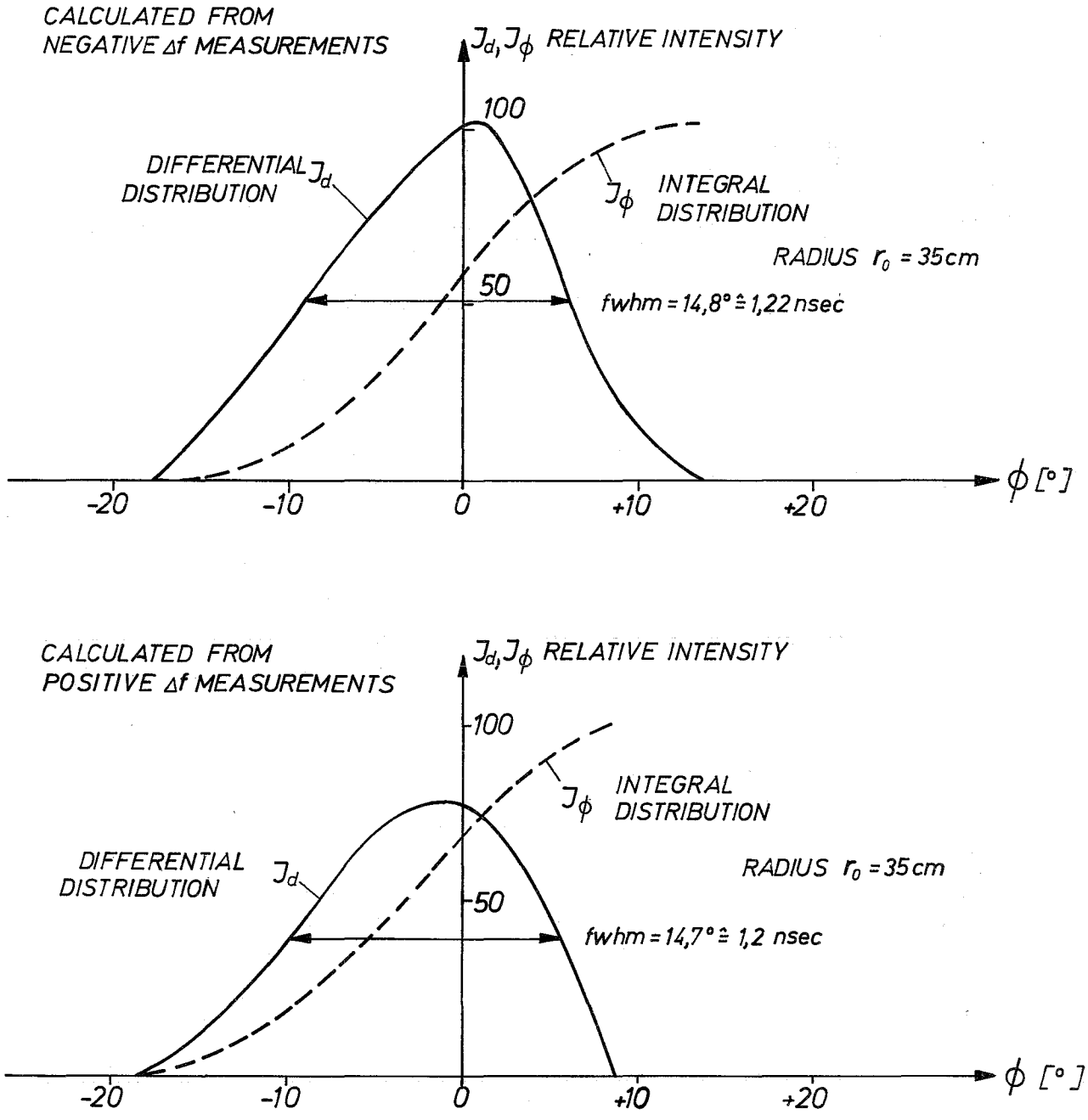
CALCULATED FROM
NEGATIVE Δf MEASUREMENTS
J_d, J_ϕ RELATIVE INTENSITY
100
DIFFERENTIAL DISTRIBUTION J_d
J_ϕ INTEGRAL DISTRIBUTION
RADIUS r_0 = 35cm
50
fwhm = 14,8° ≙ 1,22 nsec
-20
-10
0
+10
+20
ϕ [°]
CALCULATED FROM
POSITIVE Δf MEASUREMENTS
J_d, J_ϕ RELATIVE INTENSITY
100
J_ϕ INTEGRAL DISTRIBUTION
DIFFERENTIAL DISTRIBUTION J_d
RADIUS r_0 = 35cm
50
fwhm = 14,7° ≙ 1,2 nsec
-20
-10
0
+10
+20
ϕ [°]

Fig. 3.6

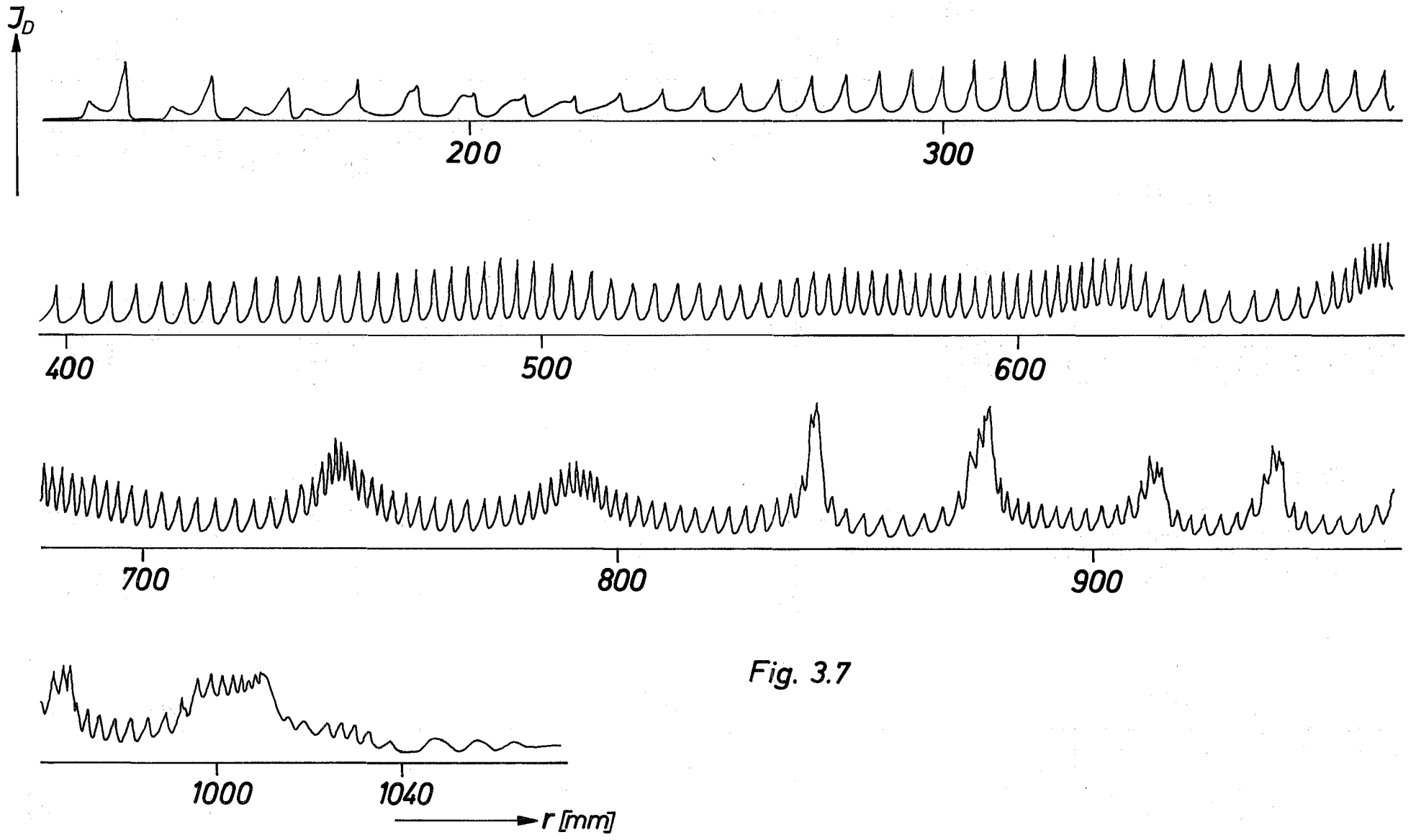

Fig. 3.7

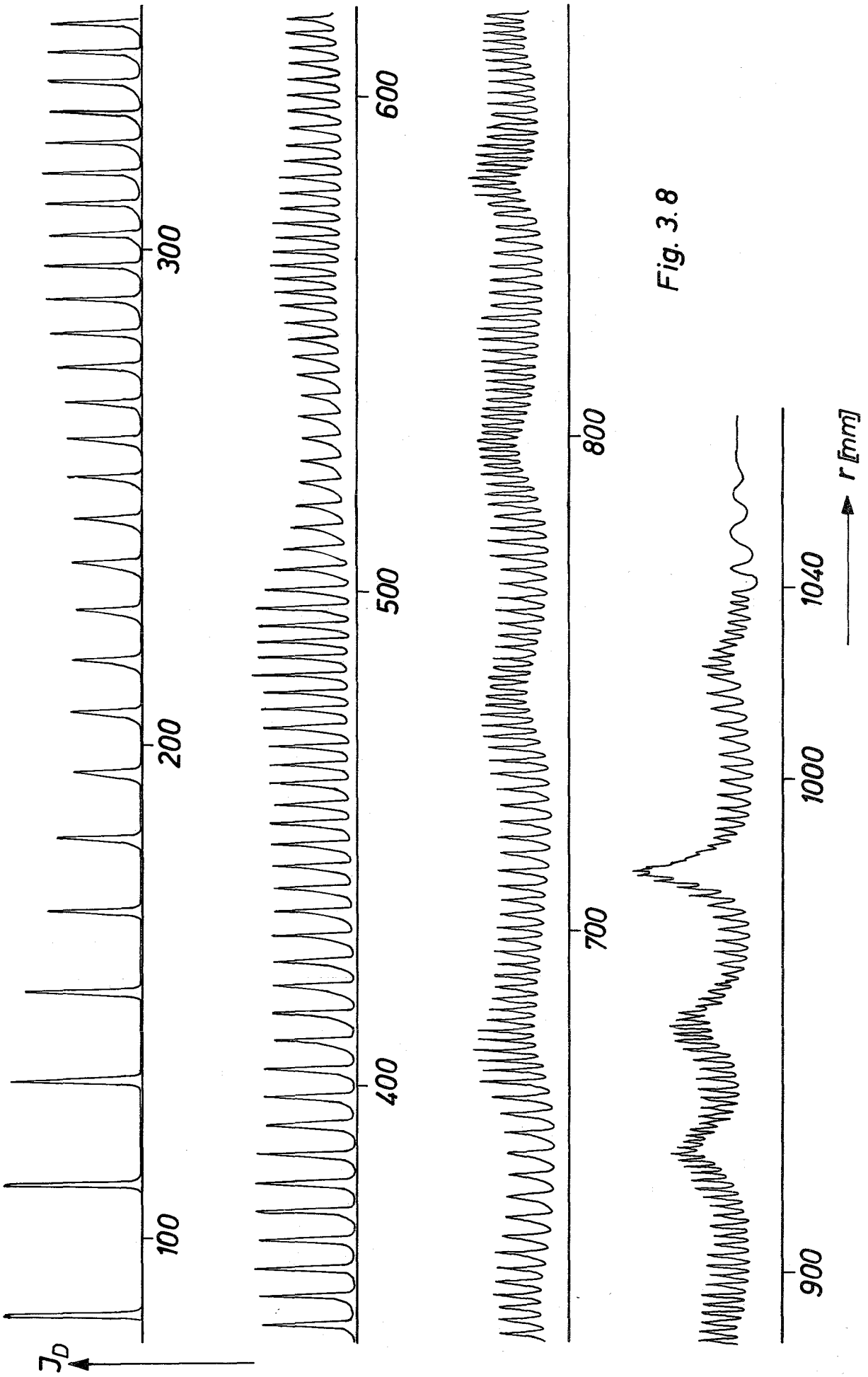

Fig. 3.8

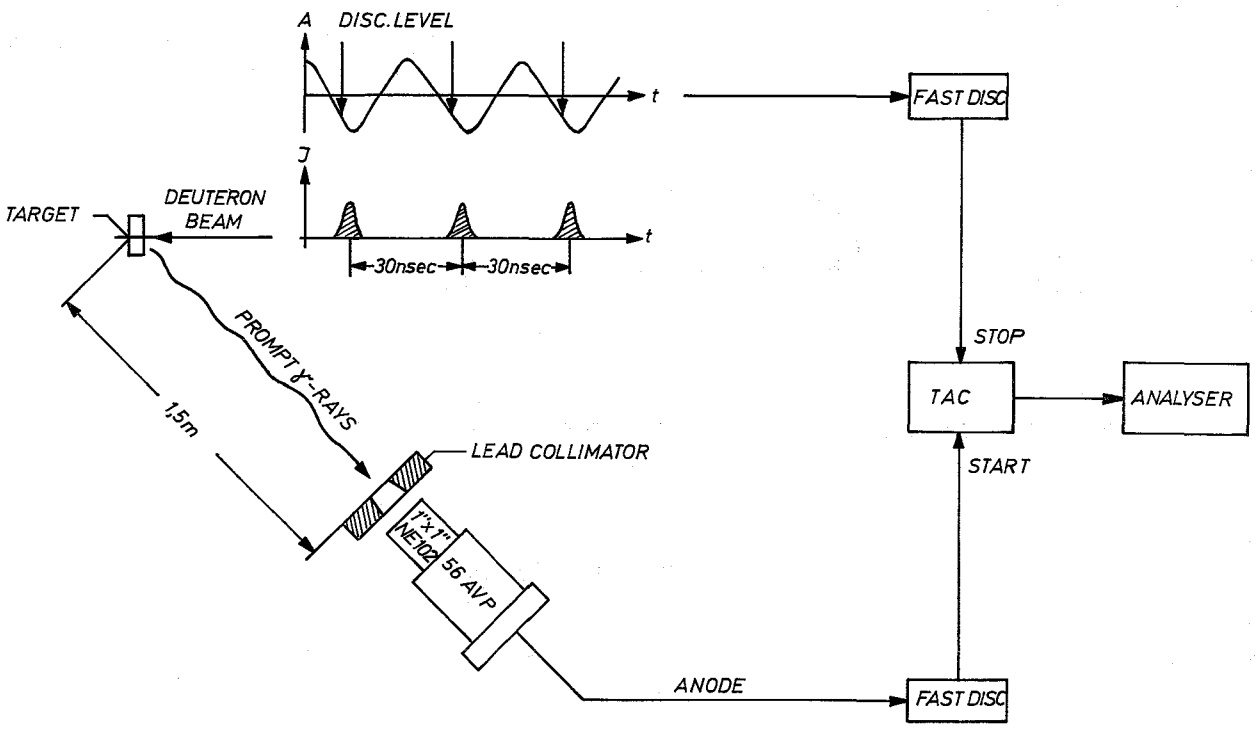

Fig. 3.9

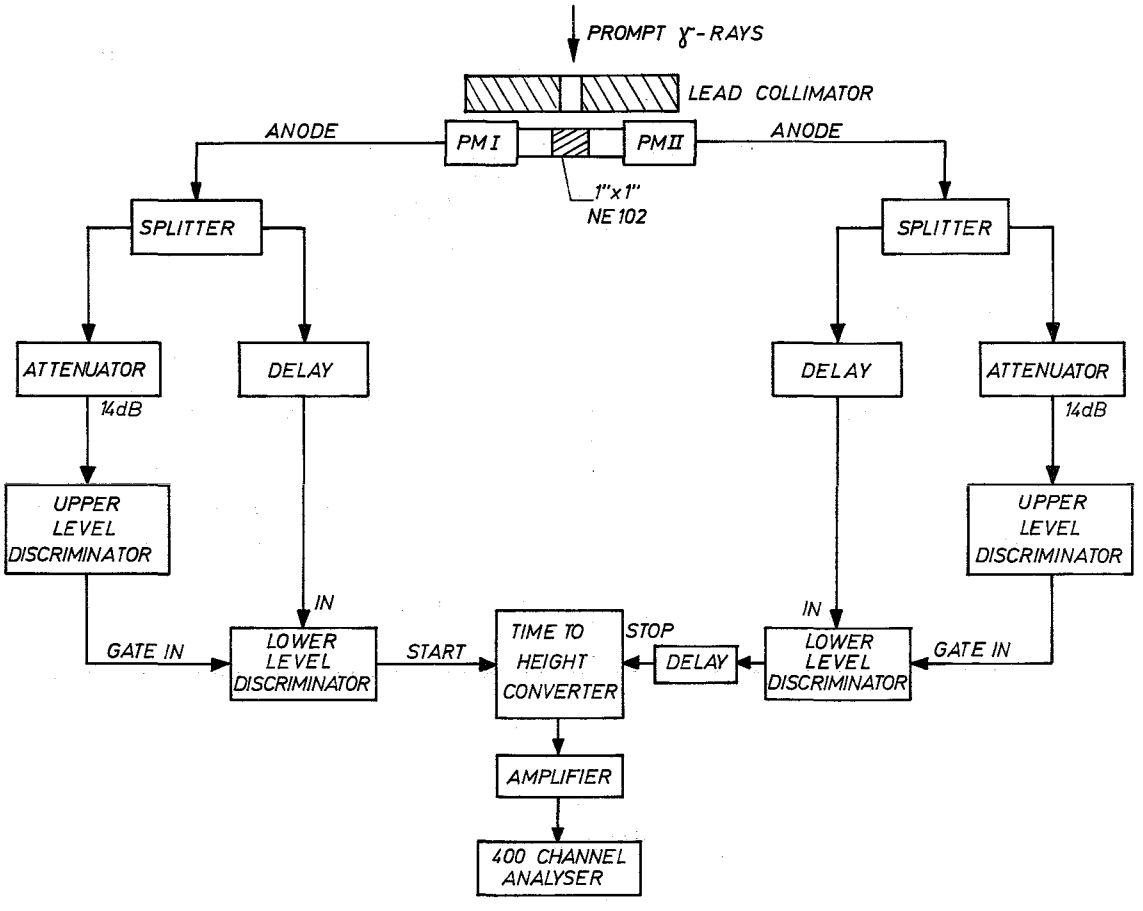

Fig. 3.10

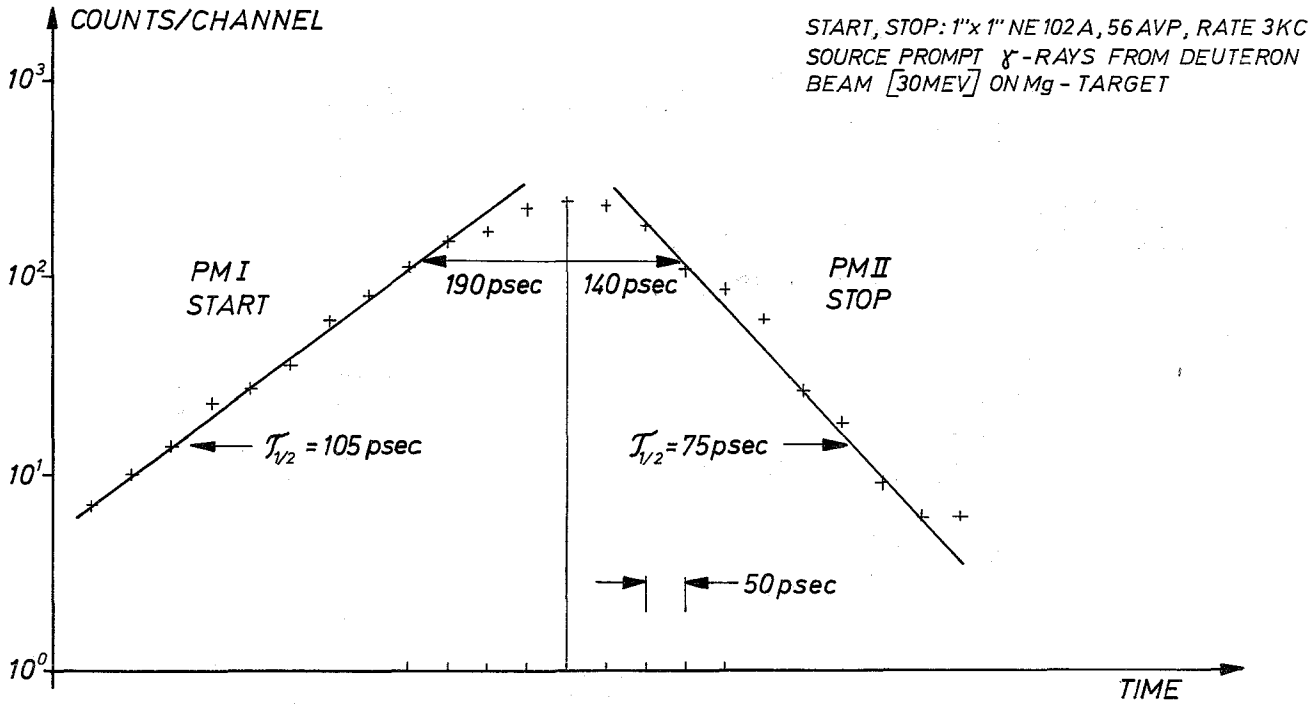

Fig. 3. 11

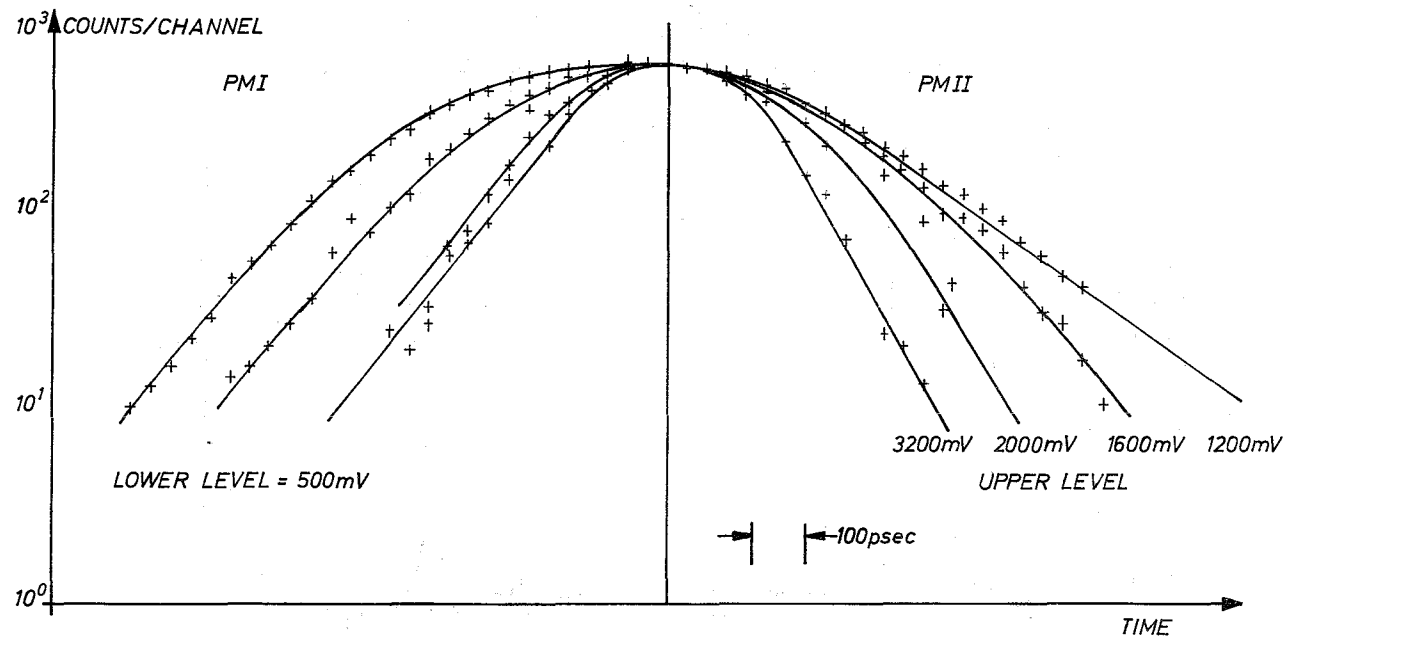

Fig. 3. 12

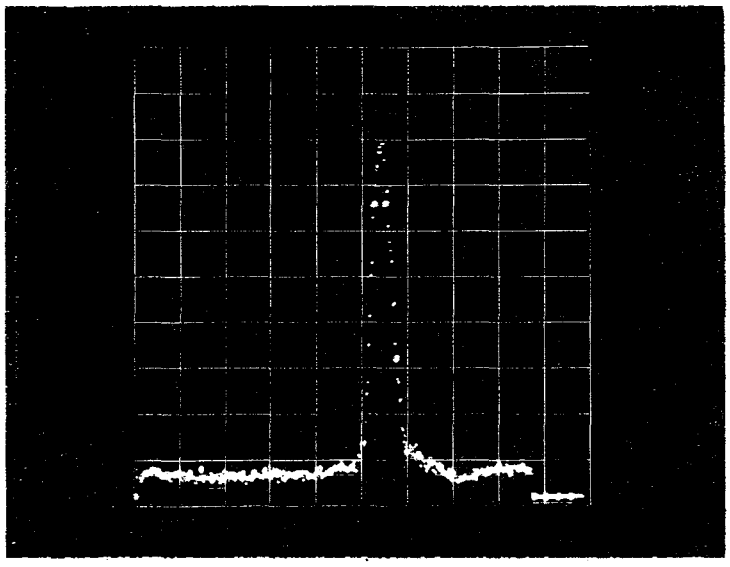

Fig. 3.13

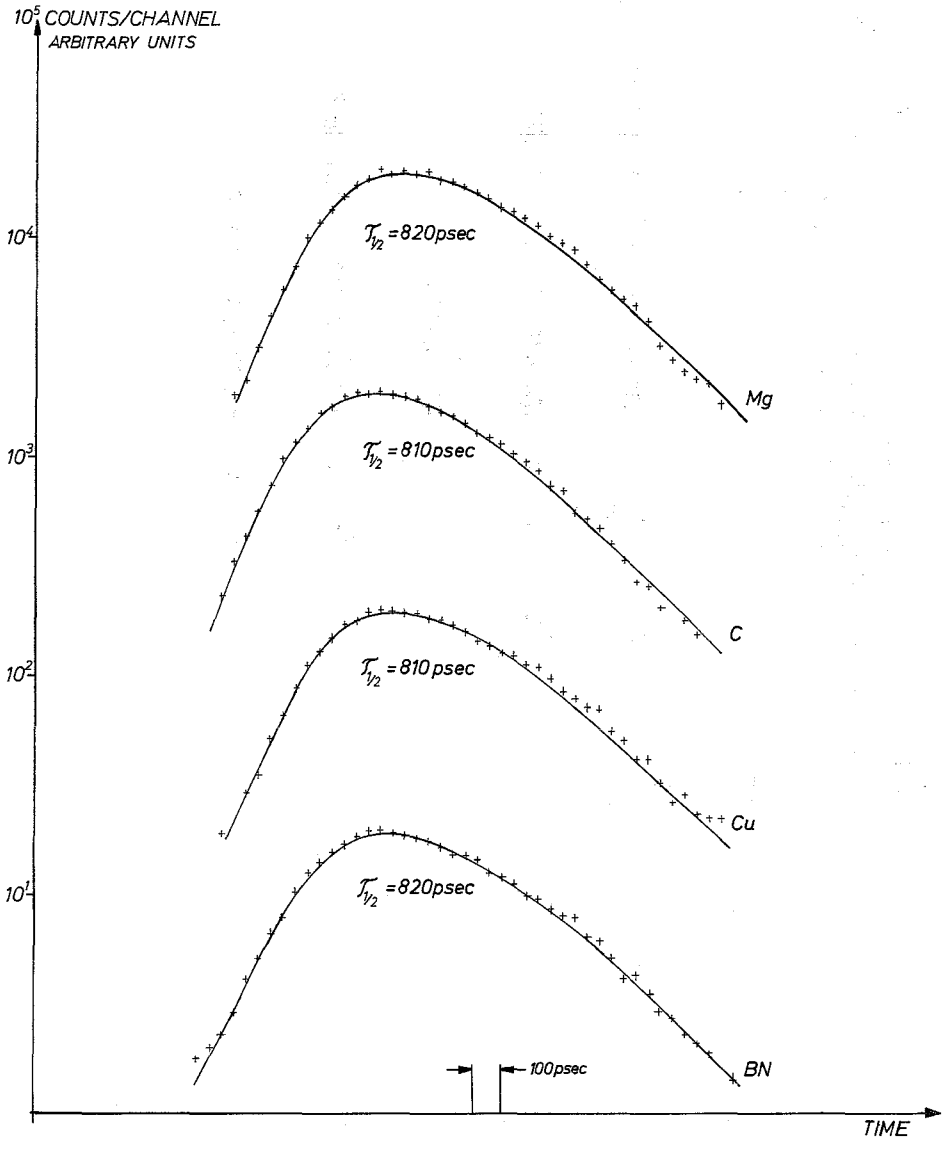

Fig. 3.14

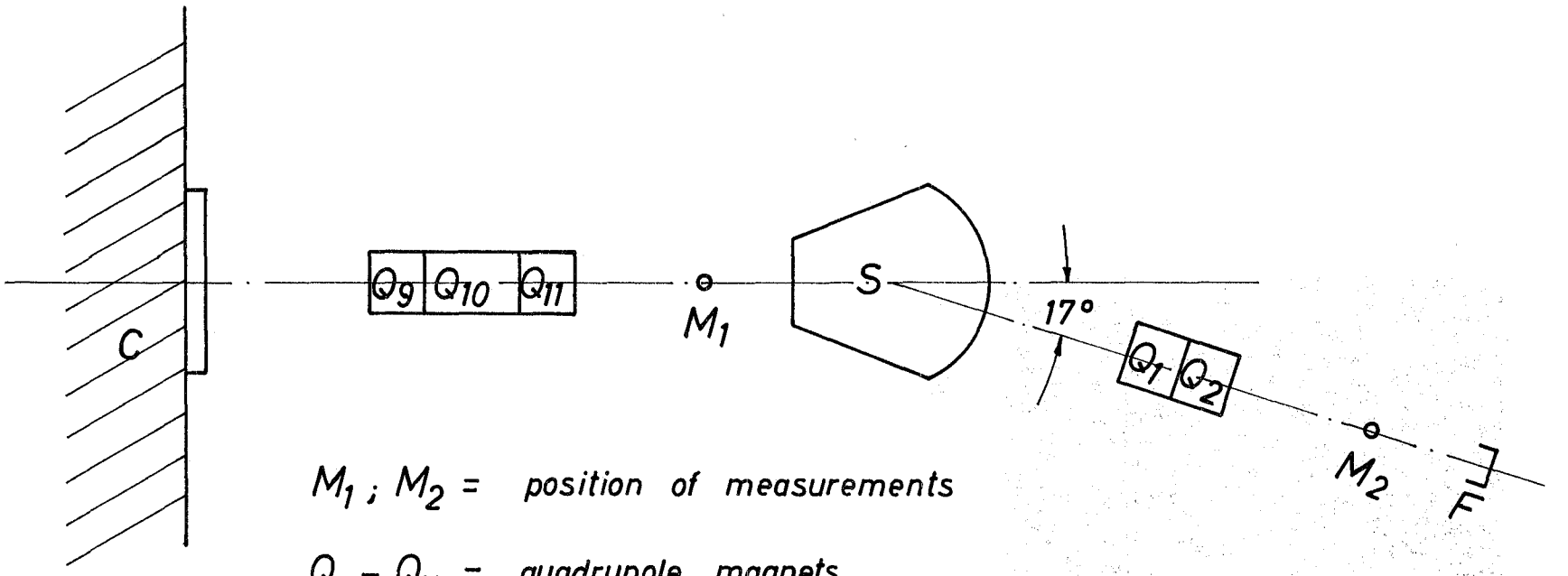

M_1 ; M_2 = position of measurements

$Q_1 - Q_{11}$ = quadrupole magnets

C = cyclotron

S = switching magnet

F = Faraday cage

Fig. 4.1

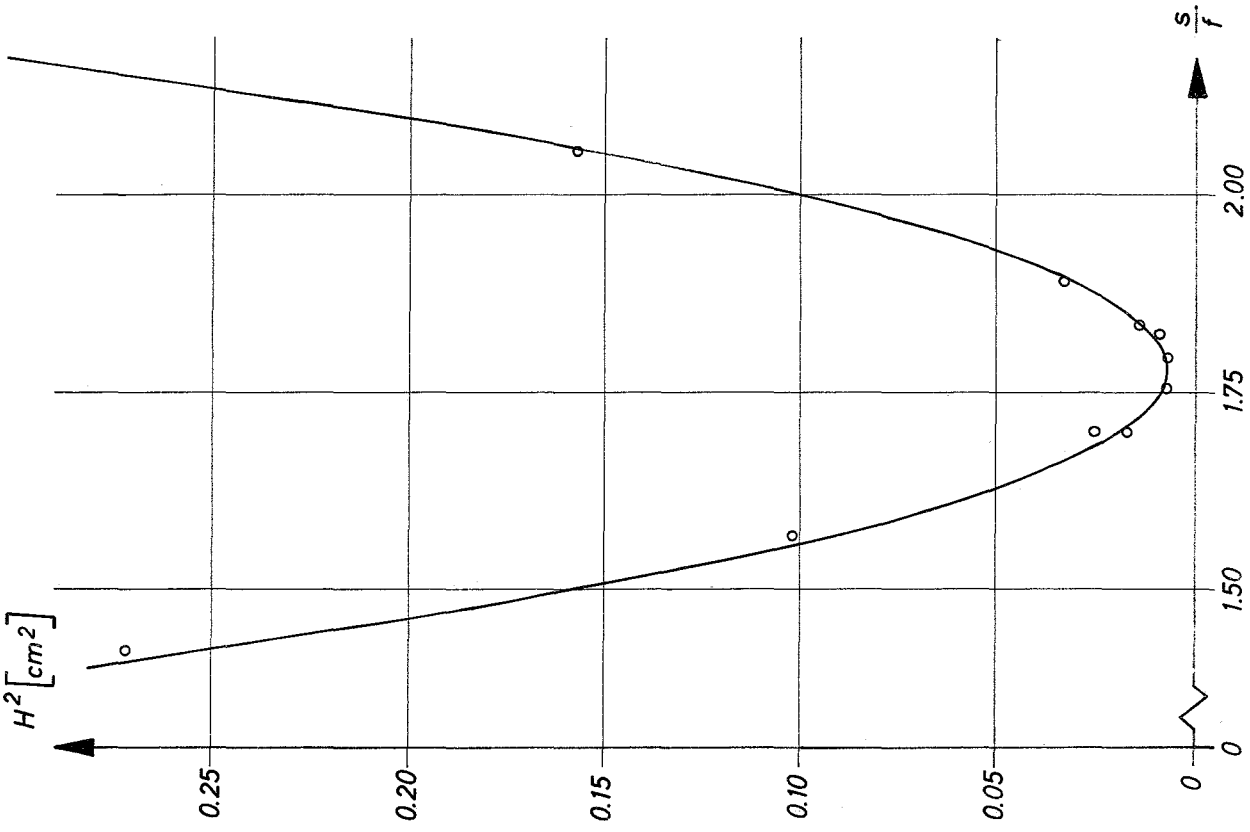

Fig. 4.2 b

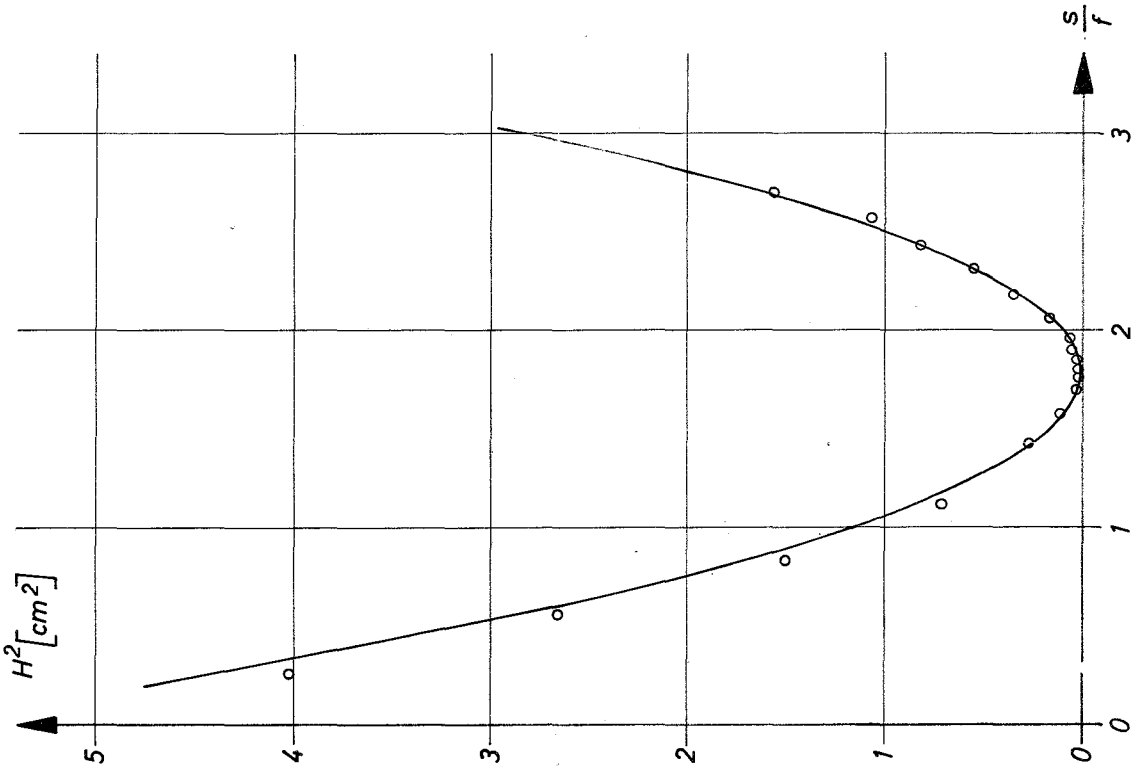

Fig. 4.2 a